Evaluating Variations of Strains in Geocell under Freeze-Thaw Cycles Using Distributed Fiber Optic Sensors

Yongxuan Gao
PhD Student
University of Victoria
Victoria, British Columbia
yongxuang@uvic.ca

Sanat Pokharel
Principal Engineer
Stratum Logics Inc.
Acheson, Alberta
sanat.pokharel@stratumlogics.com

Arghya Chatterjee
Engineering Manager
Stratum Logics Inc.
Acheson, Alberta
arghya.chatterjee@stratumlogics.com

Min Sun
Associate Professor
University of Victoria
Victoria, British Columbia
msun@uvic.ca

Cheng Lin
Associate Professor
University of Victoria
Victoria, British Columbia
chenglin918@uvic.ca

Paper prepared for the session SO - Advancements in Testing, Modelling and Innovation for Roadway/Embankment Materials and Geotechnical Engineering
2025 Transportation Association of Canada (TAC) Conference & Exhibition
Québec City, Québec

Abstract

In cold climates, cyclic freeze-thaw (F-T) action poses significant challenges to the mechanical stability of geocell-reinforced earth structures. Limited studies have evaluated the F-T responses of the geocell-reinforced earth structures; however, no research has reported the performance of geocell itself under F-T cycles. To fill this research gap, this study investigated the strain of novel polymeric alloy (NPA) geocells immersed in water under F-T cycles with high-resolution distributed fiber optic sensors (DFOS). Leveraging the unique capability of DFOS to provide continuous, distributed measurements of physical parameters along the optical fiber's path, it captured localized strain heterogeneity and material degradation patterns across the geocell structure. This technology provides unparalleled benefits as compared to conventional point-based and electrical measurement methods, such as strain gauges. Experimental results revealed compressive strain accumulation during the freezing phase, partial strain recovery in the thawing phase, and cumulative residual deformation across successive F-T cycles. Variations in results across measurement points highlighted spatial heterogeneity in geocell response. The findings from this ongoing study provided some insights into the material durability, while the longer-term monitoring would advance the understanding of geocell material degradation by F-T cycles, informing more resilient design and improved long-term performance predictions for geocell-reinforced earth structures.

Introduction

Freeze-thaw (F-T) cycles are natural processes causing frost heave and thaw weakening in soils, making them a primary driver of earth-structure damage in seasonal-frost regions. To mitigate the damage caused by F-T cycles, various countermeasures are employed in practice, such as installation of effective drainage systems, capillary barriers, replacement of frost-susceptible fines with granular materials, chemical stabilization of soils using cement or lime, and physical reinforcement of base and subbase layers with geosynthetics (Han and Jiang (2013)[1]; Li and Ashlock (2017)[2]; Li et al. (2019)[3]). Among these solutions, geosynthetics have been widely utilized to reinforce subbase and base layers, significantly improving road performance under freeze-thaw conditions. Geocells, a specific type of geosynthetic material, have gained attention due to their effectiveness in enhancing the longevity and durability of roadways and earth structures in seasonal frost regions. Several field observations have reported the beneficial effects of geocell reinforcement on the performance of roads under cyclic F-T conditions (Henry et al. (2005)[4]; Pokharel et al. (2017)[5]; Pokharel et al. (2024)[6]; Huang et al. (2025)[7]). Similarly, the positive effects were also found in laboratory tests. Huang et al. (2021)[8] (2023)[9] (2025)[10] developed a lab-scale model test device and conducted a series of freeze-thaw plate loading tests with different controlled conditions to investigate the effects of F-T cycles on the mechanical behaviour of geocell-reinforced soils. Although these studies have enhanced the understanding of geocell reinforcing effects, they have primarily focused on changes to reinforced soil or earth structures (e.g., roads) under F-T cycles. There is a notable gap in research in terms of the performance and response of geocell material itself subjected to F-T cycles. Furthermore, the material mechanical responses are typically monitored using conventional point-based and electrical measurement methods like strain gauges, which, however, fail to obtain spatially continuous information under F-T conditions.

Among various newly developed sensing technologies, Distributed Fiber Optic Sensors (DFOS) are one of the promising tools for monitoring deformation and the overall integrity of earth structure in civil engineering (Bao and Chen (2011)[11]). When an electromagnetic wave is launched into an optical fiber, the light will be redistributed by various mechanisms in the form of Rayleigh, Brillouin or Raman scattering.

If the local temperature, strain, vibration and acoustic wave changes are relayed to (mostly via direct contact with some types of specialty glue) the optical fibers, the scattered signal in the fiber will be modulated by these physical parameters, and by measuring the changes of modulated signal, one can realize fiber sensing. Therefore, fiber optic sensors can measure physical quantities such as temperature, strain and vibration of structure of interest (Selker, J.S., et al. (2006)[12]; Sun, M.-Y. (2022)[13]). There has been increasing applications of DFOS to geotechnical engineering. Facchini et al. (2024)[14] presented latest industrial application of geosynthetic materials equipped with integrated fiber-optic sensing cables for distributed strain and temperature measurements. Soga and Luo (2018)[15] introduced utilizing DFOS as an "infrastructure nerve system" to monitor structure health. Gao et al. (2025) [16] investigated the deformation and failure mechanisms in geogrid-reinforced soil with the aid of fiber optic sensors. However, there is no research in applying DFOS in monitoring geocell or geocell-reinforced structure, particularly under F-T cycles.

To address the research gaps mentioned above, this study employed DFOS to monitor the continuous strain variation of a geocell sample submerged in water and subjected to accelerated F-T cycles. The objective of this investigation was to examine the geocell's response to F-T cycles and assess its material durability. The findings will be valuable for evaluating geocell-reinforced earth structures subjected to cyclic freezing and thawing in frost regions.

Materials and Specimen Preparation

Geocells used in this test were nano-polymeric alloy (NPA) Type-C geocells donated by PRS Geo-Technologies®. NPA is a composite polymer alloy comprised of a high-performance engineering thermoplastic with a polyolefin blend (PP, PE). The blend is immiscible with high-performance nano-polymer compound (copolymers, block copolymers, blends, and/or other combinations), which is dispersed in a polyolefin matrix. Their basic properties of the NPA geocells are given in Table 1. The geocells consist of perforated walls with the height of 150 mm and the thickness of 1.1 mm, and the opening of one cell is 245 mm in the strong axis (i.e., parallel to the welded seam) and 210 mm in the weak axis. The nominal dimensions are summarized in Table 2.

Table 1. NPA Geocell mechanical properties

Properties	Value	Test standard
Seam weld splitting strength, kN/m	19	ISO-13426-1[17]
Tensile strength, kN/m	19	ISO-10319[18]
Long-term permanent deformation at 65°C, %	3	ASTM D6992[19]
Dynamic modulus at +30°C, MPa	775	ASTM E2254[20]
Brittle temperature, °C	-70	ASTM E2254[20]
Coefficient of soil-cell friction efficiency	0.95	ASTM D5321[21]
Coefficient of thermal expansion, ppm/°C	135	ASTM E831[22]

Table 2. Geocell nominal dimensions

Properties	Nominal	Description
Distance between weld seams	±2.5%	330 mm (13 in)
Cell wall heights	±5%	150 mm (6 in)

Cell dimension (Optimal opening)	±3%	245×210 mm (9.65×8.27 in)
No. of cells/m^2	±3%	40 (32)
Standard section size	±3%	2.5×8.0 mm (8.20×26.25 ft)
Standard section area	±3%	20 m^2 (215.28 ft^2)

The DFOS used in this research is high resolution distributed fiber optic strain sensor from Luna Innovations®, which measures strain change based on naturally occurring Rayleigh scattering. By comparing the measured signal changes to known calibration curves, the sensor can provide a continuous profile of strain along the fiber's entire length. Therefore, this 5-m polyimide coated fiber provides flexible and continuous strain sensing with measuring range of ±15,000 με (micro strain) along the whole length of sensor and accuracy of ±1 με. The gauge pitches, which is the distance between each discrete points of the sensor region, can be as fine as 0.65 mm and it supports measuring rates from 0.3 to 250 Hz. The operating temperature range is -40 to 200 °C, in which the thermal expansion is calibrated with specified keys.

Test specimens were prepared by cutting a segment of geocell out of the whole geocell strip and trimmed to the required dimensions, yielding a half-cell wall section with complete junctions intact. Figure 1 illustrates how the DFOS is arranged on different sections of the geocell segment. The left part provides a schematic drawing with detailed dimensions, while the right part displays a photograph of the actual specimen. The DFOS was affixed to the geocell segment in an S-shaped configuration across both the edge and central regions to capture strain changes in both longitudinal and transverse directions across the entire sample. The DFOS was securely attached to the geocell surface using epoxy and silicone coating to ensure stability and accuracy of data collection throughout the F-T cycle. As highlighted in Figure 1, three specific gauges (A, B, and C) along the DFOS were selected for long-term monitoring. Positioned along the central axis of the geocell segment, these gauges serve as representative indicators of the overarching strain trends observed during testing.

Figure 1. Layout of geocell specimen with DFOS

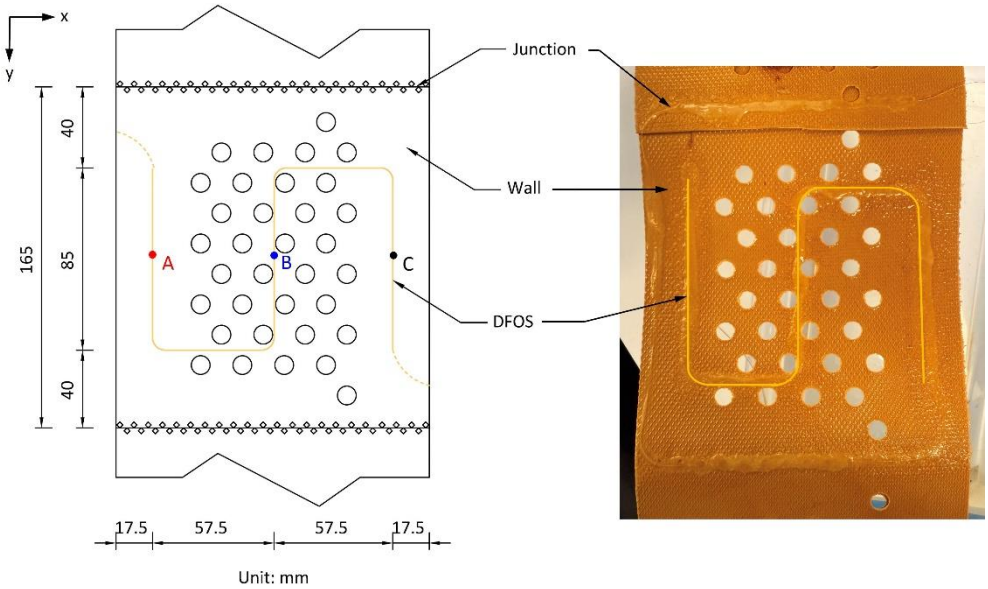

Test Procedure

This study implemented accelerated freeze-thaw (F-T) cycling to evaluate the geocell's response under repeated F-T cycles. The geocell specimen was fully submerged in distilled water within a plastic container suspending its lower face, preventing direct contact with the base, while ensuring the upper surface remained submerged to achieve uniform saturation. The specimen was soaked for 48 hours prior to testing. The water level in the container has been consistently maintained at an appropriate height. The experimental setup, including the fiber optic system and specimen in the container, is as shown in Fig 2. The fiber optic system comprised an optical distributed sensor interrogator, a connecting standoff cable, and a laptop for real-time data acquisition and storage.

Figure 2. Experimental setup of geocell strain monitoring test with fiber optic sensing system

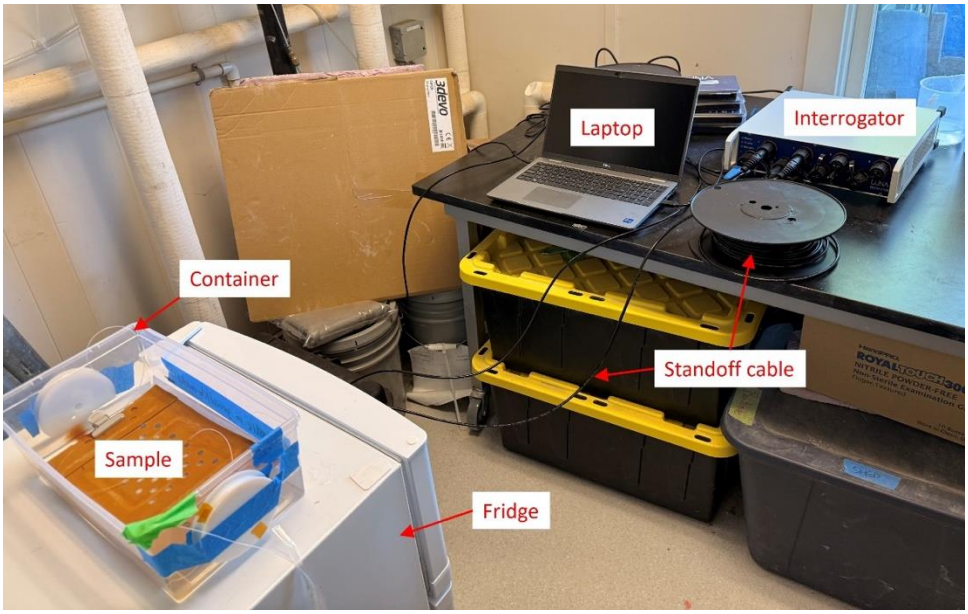

A complete freezing-thawing cycle involved two phases: freezing and thawing. During the freezing phase, the container was placed in a freezer set to and maintained at an ambient temperature of -20°C. The freezing process was halted once the container was fully frozen, and then the thawing phase began. The sample was placed outside the freezer and the room temperature was set to 20°C. The thawing process continued until the specimen fully recovered, completing one F-T cycle. Throughout the entire process, the relative humidity was kept at around 60%.

Preliminary trials were conducted to optimize phase durations, balancing complete phase transitions with minimal cycle time. Initial trials used a 6-hour freezing phase followed by an 18-hour thawing period. Critical strain thresholds were identified by analyzing gauges recording the maximum and minimum strain values during freezing and thawing. Stabilization points—defined as intervals during which strain values plateaued—were used to confirm uniform strain distribution across the geocell, indicating full phase transition. During freezing, this plateau marked the point of thermal equilibrium; during thawing, it reflected complete recovery to ambient conditions. By aligning cycle durations with these stabilization phases, the duration for F-T cycles was optimized. The optimized protocol established a 2-hour freezing

phase and a 10-hour thawing phase as the minimum effective cycle duration, which was subsequently adopted as the standard timespan for subsequent F-T cycles.

Results and Discussion

Given the extended monitoring period required for this study, the subsequent section outlines the experimental outcomes recorded across 31 freeze-thaw (F-T) cycles to date. No visible physical alterations, such as discoloration or cracking, were observed in the geocell specimen, indicating no significant structural degradation occurred during the testing phase.

Figure 3 presents the time history graphs of strain and temperature change of the geocell specimen over the 31 F-T cycles, with A, B and C representing the three designated monitoring points along DFOS as indicated in Figure 1. For one complete F-T cycle, the strain of geocell followed a distinct pattern. During the freezing stage, the geocell underwent rapid contraction, causing strain values to decrease abruptly and stabilize within a compressive strain range of -2000 to -3000 με, which was 0.2 to 0.3% contraction. Conversely, during thawing, the geocell progressively expanded, ultimately reaching a tensile strain plateau, ranging from 0 to 1000 με, which corresponded to 0 to 0.1% elongation. These strain fluctuations closely mirrored ambient temperature variations. Although discernible variations in the tensile plateaus of gauges A, B, and C emerged from the third cycle onward despite consistent ambient temperatures across each F-T cycle, the overall strain remained stable, characterized by the absence of abrupt fluctuations or deviations during intermediate phases.

Figure 3. Changes in strain and ambient temperature during F-T cycles

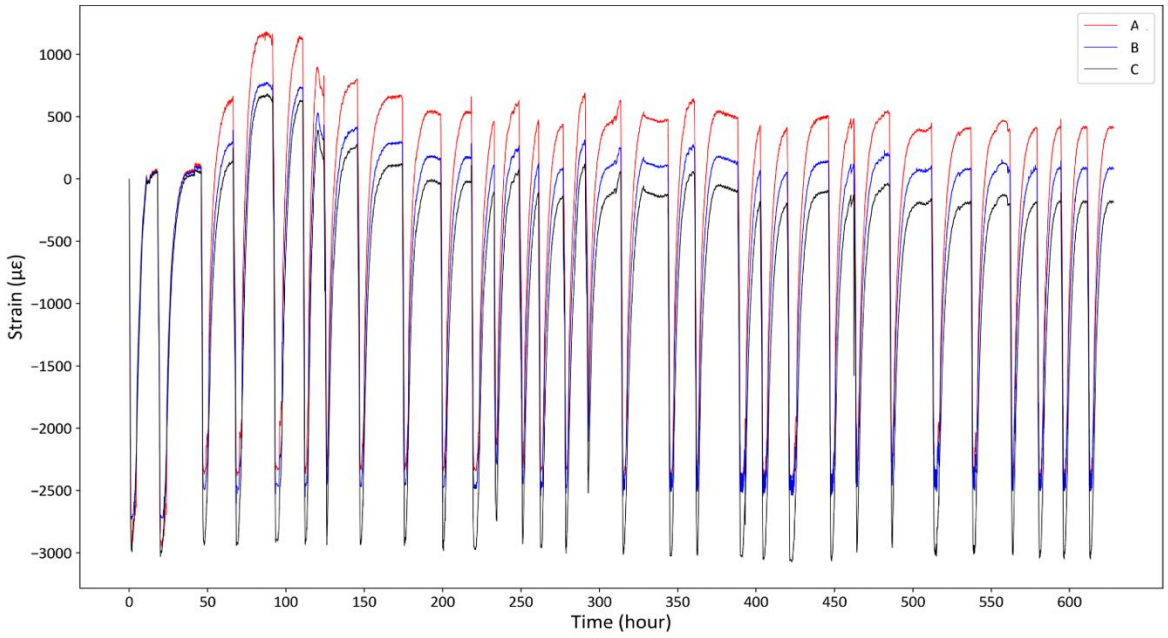

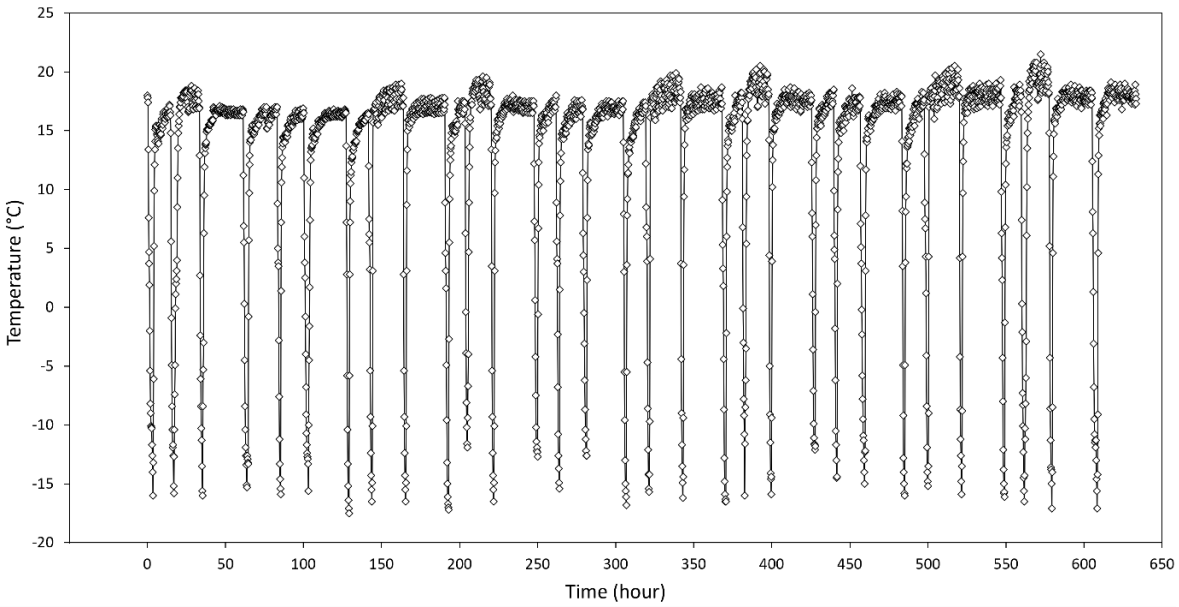

Figure 4 exhibits strain distribution patterns across three critical phases of a freeze-thaw (F-T) cycle: (1) the fully frozen state, characterized by a compressive strain plateau; (2) the thawing phase, occurring near 0 °C ambient temperature; and (3) the fully thawed state, marked by a tensile strain plateau (Figure 4(a)). For the strain contour plots, the origin (0,0) defined at the sensor's starting point. Since the freezing and thawing contour patterns are basically similar, only the plot of during thawing stage is presented. Figure 4(b) (c) and (d) presents the strain contour plots for fully frozen, during thawing and fully thawed, respectively.

The strain distribution across the geocell specimen was not uniform. The differences between maximum and minimum compressive strain at the fully frozen state and during thawing are about 1300 με (0.13%) and 600 με (0.06%) , respectively, while the difference for tensile strain at the fully thawed state is 300 με (0.03%). As highlighted in Figure 4(b), the most intensive deformation was generally concentrated at the sections of the left and right sides, where the maximum strain change occurred. It also showed an overall trend of being pulled laterally towards the edges on both sides, which can explain the divergence observed in the time history plots. Parts of DFOS in the top-right and bottom-left corners of the geocell consistently displayed minimal strain variation, likely due to their orientation or the restraining effect of nearby junctions. This can be further investigated with the results of the strain change of junction part of the geocell specimen in the future.

Figure 4. Strain distribution: (a) time history of strain change for one F-T cycle; (b) fully frozen; (c) during thawing; (d) fully thawed

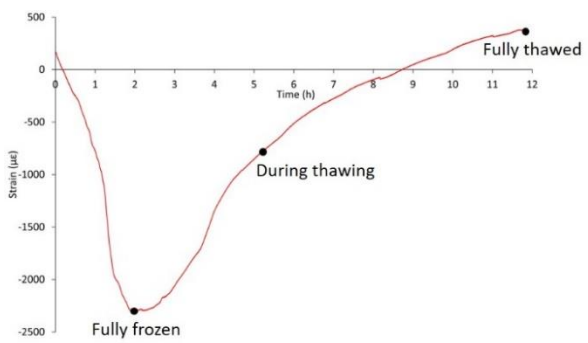

(a)

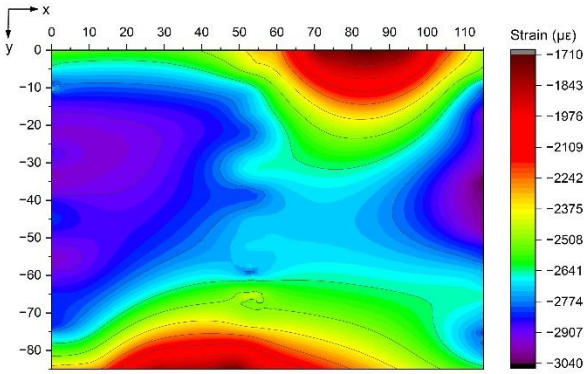

(b)

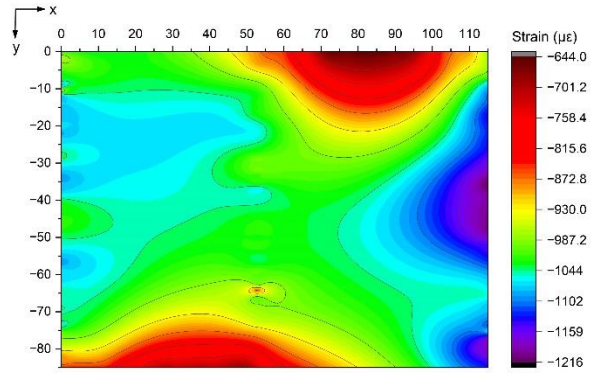

(c)

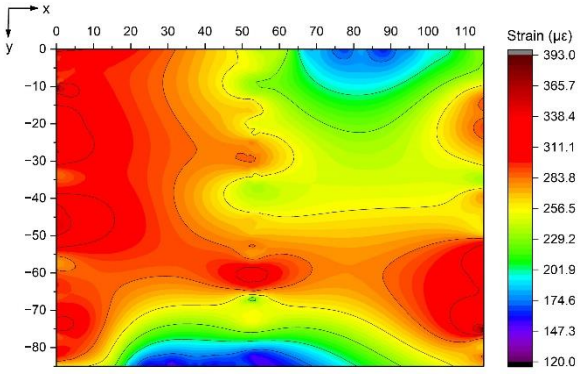

(d)

Conclusion

This study evaluated strain variations of a geocell specimen immersed in water and subjected to accelerated F-T cycles using high resolution DFOS. The time history graph of strain changes over 31 F-T cycles showed a highly repeatable strain response: rapid contraction up to 0.3% during freezing and gradual expansion up to 0.1% during thawing to a tensile plateau, closely tracking ambient temperature. Strain contour plots of one F-T cycle revealed strain change concentrated along the non-perforated side edges, producing lateral deformation toward both sides and producing the slight divergences seen in the time history curves. To date, no degradation of geocell was observed so far for this ongoing experiment. While these findings revealed the overall stability and durability of geocell material under F-T conditions, ongoing long-term monitoring is crucial to fully understand and predict material degradation. This information will inform more resilient design strategies for geocell-reinforced earth structures.

References

[1] Han, J., & Jiang, Y. "Use of geosynthetics for performance enhancement of earth structures in cold regions." *Sciences in Cold and Arid Regions*. Lanzhou: Cold and Arid Regions Environmental and Engineering Research Institute. p. 599–610. (2013)

[2] Li, C., Ashlock, J., White, D., & Vennapusa, P. "Permeability and stiffness assessment of paved and unpaved roads with geocomposite drainage layers." *Applied Sciences*. Basel: MDPI. p. 718. (2017)

[3] Li, C., Ashlock, J.C., White, D.J., & Vennapusa, P.K.R. "Mechanistic-based comparisons of stabilised base and granular surface layers of low-volume roads." *International Journal of Pavement Engineering*. London: Taylor & Francis. p. 112–124. (2019)

[4] Henry, K.S., Olson, J.P., Farrington, S.P., & Lens, J. "Improved Performance of Unpaved Roads during Spring Thaw." *Research Report.* Vicksburg, MS: US Army Corps of Engineers. (2005)

[5] Pokharel, S., Norouzi, M., Eng, P., Breault, M. "New advances in novel polymeric alloy geocell-reinforced base course for paved roads." *Innovation in Geotechnical and Materials Engineering, Conference of the Transportation Association of Canada*. (2017)

[6] Pokharel, S., Acheson, A., Dagenais, T., & Chatterjee, A. "Application of polymeric geocell reinforcement in pavements subject to freeze-thaw cycles." *Transportation Association of Canada*. Ottawa: TAC. (2024)

[7] Huang, M., Liu, J., Pokharel, S.K., Dagenais, T., Chatterjee, A., & Lin, C. "Full-scale testing and monitoring of geosynthetics-stabilized flexible pavement in Alberta, Canada." *Geotextiles and Geomembranes*. Amsterdam: Elsevier. p. 427–444. (2025)

[8] Huang, M., Lin, C., Pokharel, S.K., Tura, A., & Mukhopadhyaya, P. "Model tests of freeze-thaw behavior of geocell-reinforced soils." *Geotextiles and Geomembranes.* Amsterdam: Elsevier. p. 669–687. (2021)

[9] Huang, M., Lin, C., & Pokharel, S.K. "Freeze-thaw behavior of geocell-reinforced bases considering different fines contents." *Geosynthetics International*. London: Thomas Telford Ltd. p. 1–18. (2023)

[10] Huang, M., Pokharel, S.K., Liu, M., & Lin, C. "Freeze-thaw impacts on geocell-stabilized bases considering effects of water supply and compaction." *Geotextiles and Geomembranes.* Amsterdam: Elsevier. p. 81–95. (2025)

[11] Bao, X., & Chen, L. "Recent progress in distributed fiber optic sensors." *Sensors*. Basel: MDPI. p. 8601–8639. (2012)

[12] Selker, J.S., et al. "Distributed fiber-optic temperature sensing for hydrologic systems." *Water Resources Research.* Washington, DC: American Geophysical Union. p. W12202. (2006)

[13] Sun, M.-Y., Shi, B., Guo, J.-Y., Zhu, H.-H., Jiang, H.-T., Liu, J., Wei, G.-Q., & Zheng, X. "Development and application of fiber-optic sensing technology for monitoring soil moisture field." *Frontiers in Sensors*. Lausanne: Frontiers Media SA. p. 796789. (2022)

[14] Facchini, M., Nöther, N., & Neff, L. "Distributed fiber optic smart geosynthetics for geotechnical applications in transportation." *Procedia Structural Integrity*. Amsterdam: Elsevier B.V. p. 1597–1604. (2024)

[15] Soga, K., & Luo, L. "Distributed fiber optics sensors for civil engineering infrastructure sensing." *Journal of Structural Integrity and Maintenance*. London: Taylor & Francis. p. 1–21. (2018)

[16] Yu-Xin Gao, Hong-Hu Zhu, Jing-Wen Su, Xu-Yan Ren, Xu-Hui Guo, Hannah Wan-Huan Zhou, Bin Shi. "Experimental study on deformation and failure mechanism of geogrid-reinforced soil above voids." *Geotextiles and Geomembranes*. Amsterdam: Elsevier. p. 203-216. (2025)

[17] ISO 13426-1. "Geotextiles and geotextile-related products - Strength of internal structural junctions - Part 1: Geocells." (2019)

[18] ISO 10319. "Geosynthetics — Wide-width tensile test." (2015)

[19] ASTM D6992-16. "Standard Test Method for Accelerated Tensile Creep and Creep-Rupture of Geosynthetic Materials Based on Time-Temperature Superposition Using the Stepped Isothermal Method." *ASTM International*. West Conshohocken, PA. (2016)

[20] ASTM E2254-18. "Standard Test Method for Storage Modulus Calibration of Dynamic Mechanical Analyzers." *ASTM International*. West Conshohocken, PA. (2018)

[21] ASTM D5321/D5321M-20. "Standard Test Method for Determining the Shear Strength of Soil-Geosynthetic and Geosynthetic-Geosynthetic Interfaces by Direct Shear." *ASTM International*. West Conshohocken, PA. (2020)

[22] ASTM E831-19. "Standard Test Method for Linear Thermal Expansion of Solid Materials by Thermomechanical Analysis." *ASTM International*. West Conshohocken, PA. (2019)